McsB forms a gated kinase chamber to mark aberrant bacterial proteins for degradation

Bence Hajdusits[1a], Marcin J. Suskiewicz[1,2a], Nikolas Hundt[3,4a], Anton Meinhart[1], Robert Kurzbauer[1], Julia Leodolter[1], Philipp Kukura[3*], and Tim Clausen[1,5*]

[1] Research Institute of Molecular Pathology (IMP), Vienna BioCenter, Campus Vienna Biocenter 1, 1030 Vienna, Austria

[2] Current address: Sir William Dunn School of Pathology, University of Oxford, South Parks Road, Oxford OX1 3RE, UK

[3] Physical and Theoretical Chemistry Laboratory, Department of Chemistry, University of Oxford, South Parks Road, Oxford OX1 3QZ, UK

[4] Current address: Ludwig-Maximilians-Universität München, Department of Cellular Physiology, Biomedical Center, Großhaderner Str. 9, 82152 Planegg/Martinsried, Germany

[5] Medical University of Vienna, Vienna, Austria.

[a] These authors contributed equally.

* Correspondence should be send to Philipp Kukura, philipp.kukura@chem.ox.ac.uk; Tim Clausen, tim.clausen@imp.ac.at

Keywords

Protein quality control, targeted protein degradation, protein phosphorylation, self-compartmentalization, mass photometry.

Abstract

In Gram-positive bacteria, the McsB protein arginine kinase is central to protein quality control, labelling aberrant molecules for degradation by the ClpCP protease. Despite its importance for stress response and pathogenicity, it is still elusive how the bacterial degradation labelling is regulated. Here, we delineate the mechanism how McsB targets aberrant proteins during stress conditions. Structural data reveal a self-compartmentalized kinase, in which the active sites are sequestered in a molecular cage. The “closed” octamer interconverts with other oligomers in a phosphorylation-dependent manner and, contrary to these “open” forms, preferentially labels unfolded proteins. *In vivo* data show that heat-shock triggers accumulation of higher-order oligomers, of which the octameric McsB is essential for surviving stress situations. The interconversion of open and closed oligomers represents a distinct regulatory mechanism of a degradation labeler, allowing the McsB kinase to adapt its potentially dangerous enzyme function to the needs of the bacterial cell.

Introduction

Microorganisms have evolved specialized defense mechanisms for coping with adverse environmental changes. Pathogenic bacteria, for example, employ an intricate stress-response and protein quality control (PQC) machinery to counteract proteotoxic stresses imposed by the immune system and adapt to nutritional limitation, oxidative stress and elevated temperatures[1-4]. In Gram-positive pathogens, the repressor CtsR, the protein arginine kinase McsB and the protease ClpC:ClpP constitute the core of the stress-response operon[5-7]. The system comprises both transcriptional and post-transcriptional mechanisms, enabling the rapid expression of heat-shock factors and the elimination of damaged bacterial proteins, respectively. While the former regulatory network of transcription factors has been characterized in detail[8,9], the equally important process of removing aberrant proteins is less understood. The protein kinase McsB is critical for both processes, as it coordinates stress signaling and protein degradation pathways.

Compared to eukaryotes, bacteria express a broader range of protein-phosphorylating enzymes that target a wider spectrum of amino acid residues[10,11]. McsB is a prominent member of the specialized bacterial kinases, and has the unique activity of phosphorylating arginine residues[12]. Major substrates of McsB are the two central heat-shock repressors CtsR and HrcA[8,13]. As shown for CtsR, McsB controls the two transcription factors by phosphorylating arginine residues in their DNA-reading heads, thus promoting their dissociation from DNA and inducing the expression of stress-response genes[12,14,15]. Ultimately, de-repression of CtsR and HrcA leads to an upregulation of potent PQC factors including the McsB kinase itself, the molecular chaperones GroES and GroEL, the disaggregase ClpE and the ClpC:ClpP protease[16]. Aside from this regulatory role, the phosphoarginine (pArg) mark introduced by McsB has a broader function in the cell, serving as a degradation tag that directs client proteins to the ClpC:ClpP protease[14,17]. Impairment of the pArg-ClpC:ClpP degradation pathway precludes clearance of protein aggregates[17] and limits survival under heat-shock conditions[14]. This pArg-mediated housekeeping function is likely to underlie McsB's pivotal role as a virulence factor, enabling severe human pathogens like *Staphylococcus aureus* and *Listeria monocytogenes* to cope with adverse conditions imposed by the host immune system[18,19].

On a molecular level, the McsB kinase is composed of a specialized phospho-transferase scaffold for arginine phosphorylation and a dimerization domain aligning two subunits[20] (**Fig. 1a**). *In vitro* and *in vivo* data showed that dimer formation is a prerequisite for attaining full kinase activity, most likely by mechanistically coupling the two active sites[20]. Although the McsB dimer represents the basic functional unit of the protein arginine kinase, various oligomeric states have been reported, ranging from monomers to dimers and even higher-order oligomers[12,14,21,22]. It is not yet clear, however, whether these different oligomeric states play a role in the bacterial heat shock response. Likewise, the molecular features that enable McsB to recognize and bind protein substrates have not been resolved so far. Conceptually, the pArg mark added by McsB is similar to the eukaryotic poly-ubiquitin tag, serving as a degradation signal for general proteolysis. In eukaryotes, the ubiquitin E3 ligases, which carry out the degradation labelling, are tightly controlled enzymes, where substrate selection and/or ligase activity can be adjusted to specific physiological requirements[23]. Given its important role in deciding about the fate of bacterial proteins, the pArg-tagging activity of McsB should be carefully regulated as well. Proteomics data, however, suggest that the McsB arginine kinase is a rather promiscuous enzyme targeting a large set of substrates, without exhibiting any consensus sequence specificity[14,15,24-26]. It is thus unclear how the McsB kinase selects for aberrant proteins that need to be degraded and distinguishes these damaged molecules from natively folded proteins.

Considering the promiscuity of the McsB kinase and the existence of its different oligomeric states, we studied whether the kinase's oligomerisation status affects its function as a degradation labeller. Our in vitro and in vivo data show that oligomer conversion is critical to adapt the kinase activity of McsB to its PQC function. We found that the pArg-dependent switch in oligomeric state defines McsB's substrate specificity and becomes essential during stress situations to efficiently eliminate damaged proteins. In addition to revealing the central phospho switch that regulates degradation labeling in bacteria, our findings highlight the power of combining structural approaches with novel biophysical methodologies, which we anticipate will reveal similarly complex mechanisms in other biological systems.

Results

McsB forms higher-order oligomers in vitro and in vivo

Previous structure-function studies have been carried out with the *Geobacillus stearothermophilus* McsB kinase ($McsB_{GS}$), the prevalent model for protein arginine kinases[12,20,21,27]. $McsB_{GS}$ exists as a functional dimer, but is also capable of forming higher-order oligomers, as suggested by native mass spectrometry[20] and analytical size exclusion chromatography (SEC) data (**Extended Data Fig. 2**). To investigate the biological relevance of the various kinase states, we studied the McsB kinase from *Bacillus subtilis* ($McsB_{BS}$), which exhibits 71% sequence identity to $McsB_{GS}$. After establishing an efficient procedure for recombinant production of $McsB_{BS}$, we performed analytical SEC runs and observed a distinct distribution of oligomeric states. Whereas the profile of $McsB_{GS}$ features a sharp peak at 80 kDa, $McsB_{BS}$ lacks this dimer fraction and forms a series of larger oligomers eluting at a molecular size of 250-450 kDa (**Fig. 1b**).

To explore whether these higher-order kinase forms are present *in vivo*, we analyzed *B. subtilis* cells grown under normal and heat-shock conditions. After disrupting the bacteria, we applied the cell lysate to a SEC column, separating the bacterial proteins according to size. The Western blot profiles obtained using an McsB antibody were compared with those of recombinant $McsB_{GS}$ and $McsB_{BS}$, serving as our 80 kDa and 400 kDa size standards, respectively. This analysis indicated that cellular $McsB_{BS}$ exists in a broad range of oligomeric states including monomers, dimers and various higher-order kinase forms (**Fig. 1c**). Strikingly, $McsB_{BS}$ showed different distributions under the applied environmental settings. At standard conditions, the bulk of $McsB_{BS}$ was present as smaller oligomers, presumably monomers and dimers, whereas heat-shock induced an upregulation of markedly larger particles, which had a similar size to the in vitro reconstituted $McsB_{BS}$ protein. In sum, these data suggest that in the cell, the McsB kinase exists in different oligomeric states, which interconvert in response to changing environmental conditions.

McsB from *B. subtilis* assembles a pArg-stabilized octamer

Despite the polydispersity of the recombinant $McsB_{BS}$ sample, we initiated a structural study of it. For this purpose, we performed secondary SEC runs, enriching the peak fraction of the higher-order oligomers, and subjected this sample to crystallization trials. We obtained crystals diffracting to 2.5 Å resolution, revealing the atomic structure of the $McsB_{BS}$ octamer (**Fig. 2a**) (**Table S1**). The octameric particle represents a tetramer of dimers, with each dimer resembling the reported $McsB_{GS}$ structure in its subunit contacts, domain arrangement and active site organization (**Extended Data Fig. 3a**). The four $McsB_{BS}$ dimers form a molecular cage having the length of one dimer, 110 Å, and a diameter of 80 Å. The phosphorylation chamber has well-defined entrance gates with openings of approximately 25 Å. Potential substrates have to pass the entrance gates in order to reach the active sites, which are buried within the inner chamber (**Fig. 2b**, **Supplementary Video 1**). Notably, none of the residues implicated in substrate binding or catalysis is engaged in inter-dimer contacts, suggesting that the internal active sites are functional. Octamer formation proceeds along the extended edge of the brick-shaped McsB dimer, where two clusters of polar residues enclose a small hydrophobic core. From the polar patches, the inner contact site comprises a dense network of hydrogen bonds woven around arginine residue 194. Strikingly, the electron density revealed that Arg194 is phosphorylated at a terminal amine of its guanidinium group (**Fig. 2c**). The pArg194 phospho-guanidinium group is accommodated in a complementarily charged pocket of a neighboring dimer. This pArg receptor site (pR-RS) corresponds to the previously identified pArg binding pocket of $McsB_{GS}$ that enables allosteric stimulation[20] (**Extended Data Fig. 3b**). In the $McsB_{BS}$ octamer, Arg337*, Arg341*, and Ser285* of the molecular neighbor closely interact with the pArg194 phosphate group, whereas Asp338* tightly binds to the positively charged nitrogen of the pArg guanidinium function (**Fig. 2d**). Given these intimate ion-pair and hydrogen-bonding interactions, we presume that the pArg:pR-RS* tethering, established twice between each pair of aligned dimers, is the major interaction stabilizing the $McsB_{BS}$ octamer. Consistent with this, the pArg:pR-RS* contact accounts for half of the inter-dimer interface, which measures 850 $Å^2$. In conclusion, structural analysis of the protein arginine kinase from *B. subilits* revealed the structural organization of the McsB octamer. It assembles into a self-compartmentalized kinase stabilized by the auto-phosphorylated residue pArg194.

Although post-translational modifications have often been implicated in regulating oligomerization, the structure of the pArg194-linked McsB octamer represents, to our knowledge, the first atomic visualization of a defined higher-order oligomer that strictly depends on a specific phosphorylation event.

McsB exists in a dynamic equilibrium of monomers, dimers and multi-dimers

To better understand the change in oligomer distribution of *B. subtilis* McsB upon heat shock (**Fig. 1c**), we reconstituted the $McsB_{BS}$ system in vitro and characterized the switch mechanism using mass photometry[28]. We first studied the concentration-dependent behavior of McsB. For protein concentrations from 10 to 500 nM, we observed, in contrast to the SEC data, various small molecular weight forms including 1-, 2-, 4- and 6-mers, with the monomer and dimer being predominant at low concentrations (**Fig. 3a**). At increasing concentrations, the population shifted towards formation of higher-order oligomers, such as 4-, 6- and 8-mers. In addition, we observed small amounts of oligomers consisting of 10 and 12 subunits. When we performed mass photometry on the $McsB_{GS}$ orthologue, we observed a less complex protein mixture at lower protein concentrations (**Fig. 3b**). The kinase showed a clear preference to dimerize and started to assemble into higher-order oligomers only at higher concentrations, of about 50 nM.

Together, the single-molecule data demonstrate the co-occurrence of various McsB oligomers in a dynamic, concentration-dependent equilibrium (**Fig. 3c**). Whereas the octamer, as revealed by the crystal structure, represents a defined and rigid arrangement stabilized by pArg194, the remaining oligomers are likely to be more heterogeneous in their intermolecular contacts. In this regard, McsB has been shown to modify numerous arginine residues on its own surface[14,15,24,26]. Each of these phospho sites could potentially bind to the pArg-binding pocket of an adjacent McsB dimer to mediate oligomerization. In contrast to the caged 8-mer, these loosely linked, irregular $McsB_{BS}$ assemblies should exist as “open” kinase forms, in which the active sites are freely accessible. The large number of oligomers identified here is unprecedented among protein kinases and points to a complex enzymatic system, regulating the pArg labeling function. Moreover, the overall distribution of $McsB_{BS}$ and $McsB_{GS}$ oligomers suggest that the formation of multi-dimer assemblies is a common

property of this kinase class that might be fine-tuned in evolution to match conditions encountered by various bacterial species.

McsB oligomers interconvert in a pArg-dependent manner

The crystal structure of $McsB_{BS}$ implies that octamer formation depends on a specific pArg residue, pArg194, which could serve as a phospho-switch controlling protein assembly. To explore the impact of arginine phosphorylation on the stability of the various McsB forms, we incubated the protein samples with YwlE, a pArg-specific phosphatase[27]. We used $McsB_{BS}$ at a concentration of 500 nM, where we could observe 2-, 4-, 6-, 8- and 10-mers. Upon prolonged incubation with the YwlE phosphatase, we found that higher-order oligomers disappeared while, in parallel, the dimer fraction increased (**Fig. 3d**). A notable exception is the McsB octamer, which could not be destabilized by the YwlE phosphatase. These mass photometric data are consistent with the crystal structure of the octamer, where the pArg194 phospho-clamp is deeply buried in the molecular cage and thus inaccessible to YwlE (**Extended Data Fig. 4**). To confirm the specific shielding of pArg194, we performed an MS analysis of the YwlE-treated sample, monitoring the phosphorylation status of every McsB arginine residue individually. In accordance with the crystal structure, all pArg residues, except pArg194 and the adjacent pArg190, were quantitatively dephosphorylated (**Fig. 3e**). The resistance of McsB octamers to dephosphorylation likely also reflects their stability. Each McsB dimer in the octamer is bound to two other molecules and is thus stabilized compared to irregular multi-dimers, where most units are tethered by single pArg:pR-RS linkages. The high stability of the octamer should limit transient dissociation, which might be a prerequisite for dephosphorylation.

To further explore the stability of the octamer, we analyzed the effect of pArg as a competitive inhibitor of McsB oligomer formation. Given the dynamic interchange of McsB units, we reasoned that free pArg competes with auto-phosphorylated molecules for binding to the pR-RS, thus disturbing the polymerization of McsB dimers. To test this prediction, we incubated auto-phosphorylated McsB with free pArg using concentrations from 0.01 to 5 mM. The addition of pArg selectively destabilized the irregular $McsB_{BS}$ oligomers, as seen for the tetramer and hexamer (**Fig. 3f**). Overall, free pArg shifted the equilibrium towards the isolated monomer and dimer, and to the

caged octamer. According to these data, McsB oligomer conversion can be achieved in *trans*, for example by pArg-labelled products or pArg-carrying effector proteins.

Finally, we tested whether pArg194 stabilized the octamer in a specific manner or, alternatively, induced multimerization of McsB dimers in general. For this purpose, we generated the R194K mutant, which cannot be autophosphorylated at this position. As revealed by mass photometric data, the R194K mutation selectively destabilized the McsB octamer, whereas the relative amounts of open McsB multimers, which can be linked by other pArg sites, were not affected (**Fig. 3g**). Moreover, a SEC analysis revealed that mutating the pArg receptor site (R337A/D338A mutant) resulted in destabilization of McsB multimers, such as 4-, 6- and 8-mers, leading to an accumulation of the dimeric kinase (**Extended Data Fig. 5**).

Together, these data indicate that interconversion of McsB oligomers is a pArg-dependent process. Binding of exposed pArg residues to the pR-RS of a molecular neighbor connects McsB dimers to multimers ranging in size from 2- to 12-mers. Among the tethering pArg residues, pArg194 obtains a special role as this phospho residue can promote assembly of the closed octameric cage. In contrast to other higher-order oligomers, the self-compartmentalized octamer persists in the presence of the YwlE phosphatase and pArg-linked effector molecules. We thus presume that *in vivo*, the McsB monomer, dimer and octamer represent the functionally prevalent states of the PQC kinase.

McsB dimer and octamer have distinct kinase properties

The shift in equilibrium between open and closed $McsB_{BS}$ oligomers could represent a functional switch controlling McsB activity. To study the proposed switch in kinase function, we had to reconstitute the octamer and dimer species of the *B. subtilis* $McsB_{BS}$, and study the two forms separately. Prompted by the mass photometry results, we applied a “nano-molar” biochemical approach and diluted the $McsB_{BS}$ sample, containing higher-order McsB forms, to a final concentration of 50 nM, thereby favoring the formation of monomers and dimers (**Fig. 4a**). The diluted sample was incubated with the YwlE phosphatase. After dephosphorylating all accessible pArg residues, McsB was concentrated, applied to a SEC column, and the dimeric and octameric kinase separated (**Fig. 4a, right panel**).

Using the isolated McsB$_{BS}$ forms, we performed radiometric assays monitoring phosphorylation of β-casein, our model substrate. Though the octamer showed residual activity against casein, the activity of the dimer was 4-fold higher, revealing the preferential targeting of casein by the McsB$_{BS}$ dimer (**Fig. 4b**). To further confirm these data, we performed a "dilution-series" kinase assay, in which McsB$_{BS}$ was sequentially diluted from 1000 to 50 nM (**Fig. 4c**). To compensate for the different amounts of the kinase, the enzyme assays were prolonged for various times, ranging from 10 to 200 minutes. As clearly seen for the casein substrate, McsB gains activity upon dilution. We could only observe substrate phosphorylation when using McsB$_{BS}$ at 50 nM concentration, where oligomers fall apart into dimers (**Fig. 3a**). These data suggest that a change in oligomeric state is directly coupled with a switch in the substrate specificity of the protein kinase.

The octamer of McsB imposes a substrate filter to the kinase function

Because the McsB$_{BS}$ dimer and octamer exhibited distinct activities against casein, we next extended our analysis to further model substrates. We reasoned that the self-compartmentalized octamer may select for small and unfolded proteins, whereas the dimer may function as a promiscuous kinase. To test this hypothesis, we used a set of model proteins differing in size from 10 to 100 kDa, and representing largely folded, partially folded and unfolded proteins. We first investigated relatively small proteins, in the range of range of 12-25 kDa, showing different degrees of compactness. Radiometric kinase assays revealed that for v-Myc (bHLHZip domain, 12.5 kDa, largely unfolded), the octamer exhibited a higher phosphorylation activity than the dimer. For ComK (*B. subtilis* transcription factor of 20 kDa, partially unfolded), the octamer and dimer exhibited comparable kinase activities, and for β-casein (25 kDa, disordered but can oligomerize via interprotein β-sheets), the dimer had a 4-fold higher kinase activity as compared to the octamer (**Fig. 5a**). Of note, it has previously been shown for another protein cage, the 26S proteasome, that only the N- but not the C-terminus of β-casein can pass through a narrow entry pore[29]. A similar mechanism for the McsB octamer, might explain the inefficient modification of β-casein by this oligomer compared to the open dimer. We next studied the phosphorylation of a large, 100 kDa model protein, UNC-45 from *Caenorhabditis elegans*. For UNC-45, variants have been developed that differ in size and foldedness and were used to characterize

the quality-control E3 ligase UFD-2[30]. Compared to the $UNC45_{wt}$ wild-type protein, the $UNC45_{core}$ mutant just comprises the stably folded core region and lacks the intrinsically unstable UCS domain. The dimeric $McsB_{BS}$ was capable of phosphorylating both UNC45 variants (**Fig. 5b**). In contrast, the octameric kinase preferentially targeted the full-length construct harboring the disordered UCS domain, whereas the labeling of $UNC\text{-}45_{core}$ was very inefficient. In fact, when comparing all tested model substrates, the difference in substrate selectivity was most pronounced for the compact $UNC45_{core}$ protein, which was almost exclusively targeted by the McsB dimer. According to these data, the dimer and octamer of the McsB kinase have complementary substrate specificities. Whereas the dimer phosphorylates proteins in a rather unspecific manner, the octamer preferentially targets unfolded proteins that can pass its narrow entrance gates and enter the kinase chamber.

McsB octamer formation is crucial for coping with proteotoxic stress conditions

Our in vivo data indicated that McsB oligomers interconvert in a cell-state specific manner, with higher-order oligomers being enriched under stress conditions (**Fig. 1b**). As suggested by in vitro reconstitution experiments, the induced McsB species should mainly represent the closed octamer, the only higher-order oligomer that was stable in the presence of YwlE (**Fig. 3d**). Moreover, having characterized the octamer as secured kinase that selectively targets misfolded proteins, we wanted to test the role of this particular $McsB_{BS}$ state in the bacterial stress response. To this end, we analyzed the heat-shock-related phenotype of the R194K mutation that specifically destabilized the McsB octamer, leaving the remaining oligomers intact (**Fig. 3g**). Strikingly, during heat-shock conditions, the survival of *mcsB(R194K)*-bearing cells was significantly reduced, similar to cells carrying the Δ*mcsB* deletion. After a 2-hour incubation at 53ºC, Δ*mcsB* and *mcsB(R194K) B. subtilis* cells suffered severely, as reflected by the strongly reduced number of colony-forming units (CFUs). Whereas 60% wildtype cells survived the imposed heat shock, only 1 to 5% of the Δ*mcsB* and *mcsB(R194K)* mutant cells were thermotolerant (**Fig. 6a**), highlighting the functional importance of the pArg194-mediated switch in oligomeric state. Overall, the *in vivo* data suggest that the pArg labeling activity of the caged octamer is critical for the PQC function of McsB.

Discussion

The present study examines the regulation of the bacterial PQC factor McsB, a protein arginine kinase marking proteins for degradation by the ClpCP protease[14,20]. Our data reveal a distinct targeting mechanism for damaged proteins that is mediated by a controlled, phosphorylation-dependent switch in the oligomeric state of McsB. The complexity we have revealed in the McsB system highlights the power of combining traditional structural approaches with novel biophysical methods. While the crystal structure of the octameric McsB provided the molecular framework for studying the phospho switch that coordinates kinase assembly, mass photometry was crucial for illuminating the heterogeneity of McsB samples and, ultimately, the importance of oligomeric interconversion for function and regulation. McsB is just one example of the many dynamic protein complexes in the cell, most of which exhibit a remarkable versatility in forming functionally distinct assemblies. We thus predict that similar complexity and non-covalent dynamics exist in other biological systems, which are now amenable to the integrative structural and biophysical approaches outlined here.

How do the new findings impact on the function of McsB in the cell? So far, it has been established that McsB constitutes together with ClpC and ClpP the core of the stress response system in Gram-positive bacteria, as also reflected by the thermosensitive phenotype of Δ*mcsB* cells (**Fig. 6a**). In the bacterial PQC system, McsB has to accomplish two important tasks. First, at the onset of the stress response, McsB phosphorylates and inactivates the transcriptional repressors CtsR and HrcA, thereby inducing expression of heat-shock genes, including McsB itself. Our data suggest that the increased levels of McsB induce the formation of higher-order oligomers of McsB with enhanced phosphorylation activity. On the other hand, autophosphorylation of McsB is counteracted by the phosphatase YwlE. Thus, the elevated McsB protein levels should ultimately lead to the enrichment of the closed octamer (**Fig. 6b**), which we show to be the active kinase species responsible for labelling aberrant proteins for degradation. Once the stress stimulus ends, the protein levels of McsB decrease to a level where disassembly of the octamer is favored. Dephosphorylation by YwlE should then cause McsB to shift back to its monomeric and dimeric forms, the kinase states shown to be prevalent in non-stressed bacteria. While the monomer is enzymatically inactive and may provide a cellular pool of activatable McsB units, the dimer is expected to execute the basal housekeeping activity, with its kinase activity against

folded proteins being counteracted by the YwlE phosphatase. Overall, these findings highlight the fine balance in PQC factor activity as required for efficient thermotolerance and to cope with adverse environmental conditions. Our data show that degradation labeling is as carefully regulated in bacteria as it is in eukaryotes. In eukaryotes, ubiquitin E3 ligases are under the control of a variety of measures including the use of adaptor proteins, changes in oligomeric composition and intricate conformational switches[31-33]. Similarly, the McsB kinase exists in open and closed forms with characteristic substrate preferences, allowing rapid adjustment of its E3-like labeling activity in response to proteotoxic stresses.

Key to controlling McsB is the cage-like organization of the octamer it forms. As visualized by a high-resolution crystal structure, the active sites are sequestered in an internal phosphorylation chamber that is only accessible through lateral entry gates. McsB thus belongs to the family of self-compartmentalized PQC factors, featuring a structural organization similar to that in higher-order proteases, such as the proteasome[34], ClpP[35] and DegP[36]. In these complexes, the buried active sites cannot be accessed by natively folded proteins. Intricate gating and activation mechanisms prevent unwanted action on non-cognate proteins, ensuring the tight control of otherwise dangerous proteolytic machines[37-39]. Similarly, in the McsB octamer, the small size of the entry gate, which is only 25 Å wide, constitutes a molecular filter favoring the phosphorylation of unstructured polypeptides. Consistent with this, we observed that the caged kinase phosphorylates unfolded proteins in a highly selective and efficient manner. The functional importance of the described McsB phosphorylation chamber is highlighted by the thermosensitive phenotype of the R194K mutation, which impairs octamer stability rather than enzymatic function. To our knowledge, such a strong in vivo phenotype caused by destabilizing a distinct oligomeric state has not been reported for any other PQC factor. We presume that small-molecule compounds blocking octamer formation will abolish the bacterial stress response and cause deleterious effects, as exemplified here for the R194K mutant. Targeting the oligomer conversion of McsB - which is mediated by a single phosphate group - thus represents an appealing strategy to develop novel antibiotics, interfering with an essential step in the PQC system of bacterial pathogens.

Acknowledgements

We thank all members of the Clausen group, in particular Sabryna Junker, Julian Ehrmann and Renato Arnese, for remarks on the manuscript and discussions. We thank Catherine Lichten for critical reading of the manuscript. We are grateful to Robert Konrat, Borja Mateos and Karin Leodolter for providing purified v-myc(bHLHZip) protein and to the staff at the ESRF (Grenoble, France) and SLS (Villingen, Switzerland), where diffraction data were recorded. The final high-resolution data set was collected at the SLS beamline X06SA. Atomic coordinates and structure factors of the $McsB_{BS}$ crystal structure have been deposited at the Protein Data Bank (PDBe) under accession code 6TV6. This work was supported by a grant from the European Research Council (AdG 694978, to T.C. and CoG 819593 to P.K.) and by FFG Headquarter Grant 852936 (to T.C.). The IMP is supported by Boehringer Ingelheim.

Author contributions

P.K. and T.C. designed experiments; B.H. and M.J.S. purified McsB and performed biochemical assays; B.H. and R.K. prepared bacterial strains and carried out the in vivo analysis; J.L. performed the mass spectrometry analysis; N.H. the mass photometry analysis; and B.H., M.J.S, A.M. and T.C. the crystallographic analysis; T.C. coordinated the research project and prepared the manuscript with inputs from all authors.

Declaration of interests

The authors declare no competing interests.

REFERENCES

1. Rowley, G., Spector, M., Kormanec, J. & Roberts, M. Pushing the envelope: extracytoplasmic stress responses in bacterial pathogens. *Nat Rev Microbiol* **4**, 383-94 (2006).

2. Raju, R.M. et al. Mycobacterium tuberculosis ClpP1 and ClpP2 function together in protein degradation and are required for viability in vitro and during infection. *PLoS Pathog* **8**, e1002511 (2012).

3. Elharar, Y. et al. Survival of mycobacteria depends on proteasome-mediated amino acid recycling under nutrient limitation. *EMBO J* **33**, 1802-14 (2014).

4. Muller, A.U. & Weber-Ban, E. The Bacterial Proteasome at the Core of Diverse Degradation Pathways. *Front Mol Biosci* **6**, 23 (2019).

5. Derre, I., Rapoport, G. & Msadek, T. CtsR, a novel regulator of stress and heat shock response, controls clp and molecular chaperone gene expression in gram-positive bacteria. *Mol Microbiol* **31**, 117-31 (1999).

6. Kruger, E. & Hecker, M. The first gene of the Bacillus subtilis clpC operon, ctsR, encodes a negative regulator of its own operon and other class III heat shock genes. *J Bacteriol* **180**, 6681-8 (1998).

7. Kirstein, J., Dougan, D.A., Gerth, U., Hecker, M. & Turgay, K. The tyrosine kinase McsB is a regulated adaptor protein for ClpCP. *EMBO J* **26**, 2061-70 (2007).

8. Schumann, W. The Bacillus subtilis heat shock stimulon. *Cell Stress Chaperones* **8**, 207-17 (2003).

9. Chaturongakul, S. et al. Transcriptomic and phenotypic analyses identify coregulated, overlapping regulons among PrfA, CtsR, HrcA, and the alternative sigma factors sigmaB, sigmaC, sigmaH, and sigmaL in Listeria monocytogenes. *Appl Environ Microbiol* **77**, 187-200 (2011).

10. Mijakovic, I., Grangeasse, C. & Turgay, K. Exploring the diversity of protein modifications: special bacterial phosphorylation systems. *FEMS Microbiol Rev* **40**, 398-417 (2016).

11. Macek, B. et al. Protein post-translational modifications in bacteria. *Nat Rev Microbiol* **17**, 651-664 (2019).

12. Fuhrmann, J. et al. McsB is a protein arginine kinase that phosphorylates and inhibits the heat-shock regulator CtsR. *Science* **324**, 1323-7 (2009).

13. Schumann, W. Regulation of bacterial heat shock stimulons. *Cell Stress Chaperones* **21**, 959-968 (2016).

14. Trentini, D.B. et al. Arginine phosphorylation marks proteins for degradation by a Clp protease. *Nature* **539**, 48-53 (2016).

15. Schmidt, A. et al. Quantitative phosphoproteomics reveals the role of protein arginine phosphorylation in the bacterial stress response. *Mol Cell Proteomics* **13**, 537-50 (2014).

16. Gophna, U. & Ron, E.Z. Virulence and the heat shock response. in *International Journal of Medical Microbiology* Vol. 292 453-461 (Elsevier GmbH, 2003).

17. Stannek, L., Gunka, K., Care, R.A., Gerth, U. & Commichau, F.M. Factors that mediate and prevent degradation of the inactive and unstable GudB protein in Bacillus subtilis. *Front Microbiol* **5**, 758 (2014).

18. Wozniak, D.J., Tiwari, K.B., Soufan, R. & Jayaswal, R.K. The mcsB gene of the clpC operon is required for stress tolerance and virulence in Staphylococcus aureus. *Microbiology* **158**, 2568-76 (2012).

19. Singh, L.K. et al. clpC operon regulates cell architecture and sporulation in Bacillus anthracis. *Environ Microbiol* **17**, 855-65 (2015).

20. Suskiewicz, M.J. et al. Structure of McsB, a protein kinase for regulated arginine phosphorylation. *Nat Chem Biol* **15**, 510-518 (2019).

21. Jung, H., Choi, Y., Lee, D., Seo, J.K. & Kee, J.M. Distinct phosphorylation and dephosphorylation dynamics of protein arginine kinases revealed by fluorescent activity probes. *Chem Commun (Camb)* **55**, 7482-7485 (2019).

22. Kirstein, J., Zuhlke, D., Gerth, U., Turgay, K. & Hecker, M. A tyrosine kinase and its activator control the activity of the CtsR heat shock repressor in B. subtilis. *EMBO J* **24**, 3435-45 (2005).

23. Deshaies, R.J. & Joazeiro, C.A. RING domain E3 ubiquitin ligases. *Annu Rev Biochem* **78**, 399-434 (2009).

24. Elsholz, A.K. et al. Global impact of protein arginine phosphorylation on the physiology of Bacillus subtilis. *Proc Natl Acad Sci U S A* **109**, 7451-6 (2012).

25. Junker, S. et al. Spectral Library Based Analysis of Arginine Phosphorylations in Staphylococcus aureus. *Mol Cell Proteomics* **17**, 335-348 (2018).

26. Trentini, D.B., Fuhrmann, J., Mechtler, K. & Clausen, T. Chasing Phosphoarginine Proteins: Development of a Selective Enrichment Method Using a Phosphatase Trap. *Mol Cell Proteomics* **13**, 1953-64 (2014).

27. Fuhrmann, J. et al. Structural basis for recognizing phosphoarginine and evolving residue-specific protein phosphatases in gram-positive bacteria. *Cell Rep* **3**, 1832-9 (2013).

28. Young, G. et al. Quantitative mass imaging of single biological macromolecules. *Science* **360**, 423-427 (2018).

29. Berko, D. et al. The direction of protein entry into the proteasome determines the variety of products and depends on the force needed to unfold its two termini. *Mol Cell* **48**, 601-11 (2012).

30. Hellerschmied, D. et al. UFD-2 is an adaptor-assisted E3 ligase targeting unfolded proteins. *Nat Commun* **9**, 484 (2018).

31. Lydeard, J.R., Schulman, B.A. & Harper, J.W. Building and remodelling Cullin-RING E3 ubiquitin ligases. *EMBO Rep* **14**, 1050-61 (2013).

32. Plechanovova, A. et al. Mechanism of ubiquitylation by dimeric RING ligase RNF4. *Nat Struct Mol Biol* **18**, 1052-9 (2011).

33. Zheng, N. & Shabek, N. Ubiquitin Ligases: Structure, Function, and Regulation. *Annu Rev Biochem* **86**, 129-157 (2017).

34. Groll, M. et al. A gated channel into the proteasome core particle. *Nat Struct Biol* **7**, 1062-7 (2000).

35. Wang, J., Hartling, J.A. & Flanagan, J.M. The structure of ClpP at 2.3 A resolution suggests a model for ATP-dependent proteolysis. *Cell* **91**, 447-56 (1997).

36. Krojer, T., Garrido-Franco, M., Huber, R., Ehrmann, M. & Clausen, T. Crystal structure of DegP (HtrA) reveals a new protease-chaperone machine. *Nature* **416**, 455-9 (2002).

37. Dong, Y. et al. Cryo-EM structures and dynamics of substrate-engaged human 26S proteasome. *Nature* **565**, 49-55 (2019).

38. Gatsogiannis, C., Balogh, D., Merino, F., Sieber, S.A. & Raunser, S. Cryo-EM structure of the ClpXP protein degradation machinery. *Nat Struct Mol Biol* **26**, 946-954 (2019).

39. Krojer, T. et al. Structural basis for the regulated protease and chaperone function of DegP. *Nature* **453**, 885-90 (2008).

40. Fuhrmann, J., Subramanian, V., Kojetin, D.J. & Thompson, P.R. Activity-Based Profiling Reveals a Regulatory Link between Oxidative Stress and Protein Arginine Phosphorylation. *Cell Chem Biol* **23**, 967-977 (2016).

41. Antelmann, H. et al. Expression of a stress- and starvation-induced dps/pexB-homologous gene is controlled by the alternative sigma factor sigmaB in Bacillus subtilis. *J Bacteriol* **179**, 7251-6 (1997).

42. Kabsch, W. Xds. *Acta Crystallogr D Biol Crystallogr* **66**, 125-32 (2010).

43. McCoy, A.J. et al. Phaser crystallographic software. *J Appl Crystallogr* **40**, 658-674 (2007).

44. Emsley, P. & Cowtan, K. Coot: model-building tools for molecular graphics. *Acta Crystallogr D Biol Crystallogr* **60**, 2126-32 (2004).

45. Liebschner, D. et al. Macromolecular structure determination using X-rays, neutrons and electrons: recent developments in Phenix. *Acta Crystallogr D Struct Biol* **75**, 861-877 (2019).

46. Williams, C.J. et al. MolProbity: More and better reference data for improved all-atom structure validation. *Protein Sci* **27**, 293-315 (2018).

47. Dorfer, V. et al. MS Amanda, a universal identification algorithm optimized for high accuracy tandem mass spectra. *J Proteome Res* **13**, 3679-84 (2014).

48. Kall, L., Canterbury, J.D., Weston, J., Noble, W.S. & MacCoss, M.J. Semi-supervised learning for peptide identification from shotgun proteomics datasets. *Nat Methods* **4**, 923-5 (2007).

49. Taus, T. et al. Universal and confident phosphorylation site localization using phosphoRS. *J Proteome Res* **10**, 5354-62 (2011).

50. Cole, D., Young, G., Weigel, A., Sebesta, A. & Kukura, P. Label-Free Single-Molecule Imaging with Numerical-Aperture-Shaped Interferometric Scattering Microscopy. *ACS Photonics* **4**, 211-216 (2017).

51. Yildiz, A. et al. Myosin V walks hand-over-hand: single fluorophore imaging with 1.5-nm localization. *Science* **300**, 2061-5 (2003).

52. Loy, G. & Zelinsky, A. Fast radial symmetry for detecting points of interest. *IEEE Transactions on Pattern Analysis and Machine Intelligence* **25**, 959-973 (2003).

FIGURES

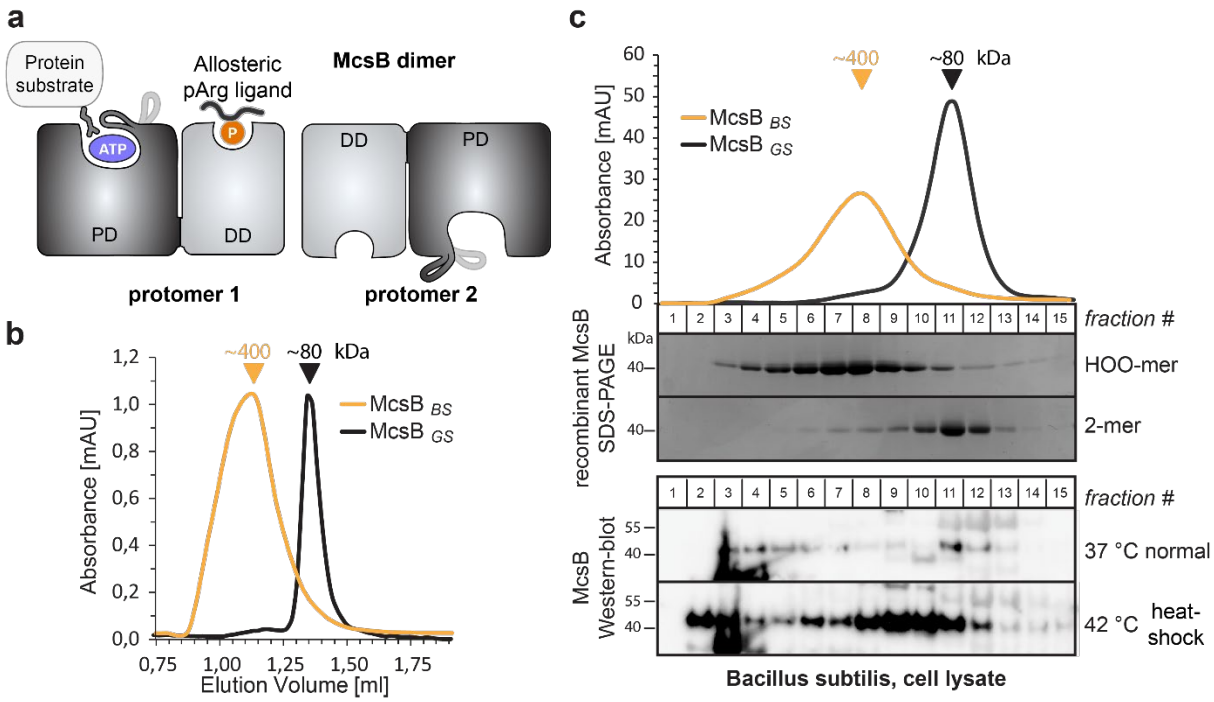

Figure 1: McsB$_{BS}$ forms higher order oligomers *in vitro* and *in vivo*.

(**a**) Schematic picture of the McsB dimer, emphasizing its domain architecture and the location of the catalytic and allosteric sites (PD, phosphotransferase domain; DD, dimerization domain). (**b**) SEC runs of McsB$_{BS}$ and purified McsB$_{GS}$ dimer. Triangular markers indicate the size of the peaks. (**c**) SEC analysis of heat-shocked and non-heat shocked *B. subtilis* cell lysates. Comparing the Western blots with blots of isolated dimeric and higher-order McsB reveal the different distributions of oligomers under the applied conditions.

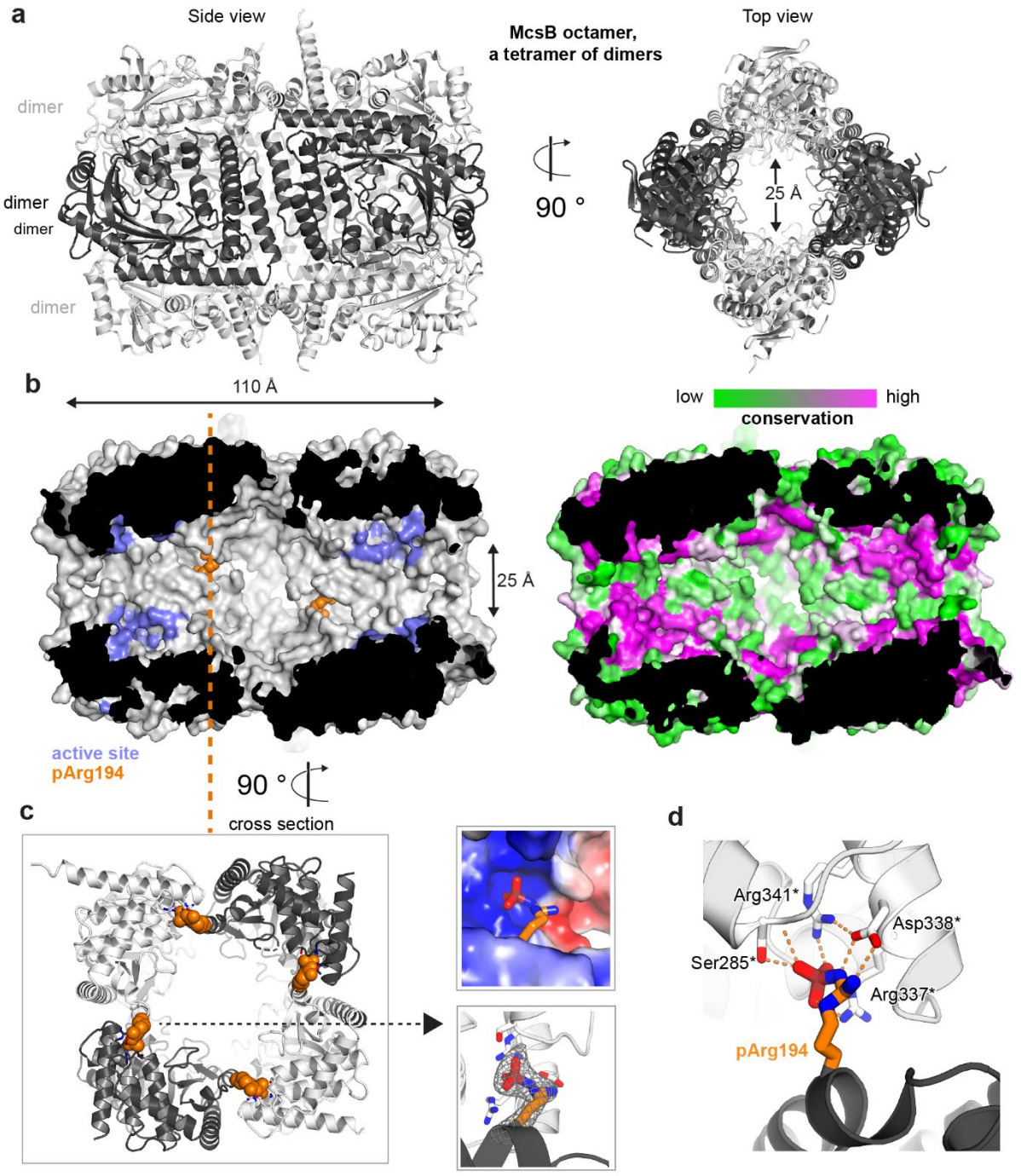

Figure 2: Crystal structure of the McsB$_{BS}$ octamer

(a) Ribbon plot of the McsB$_{BS}$ octamer (side and top views) with alternating dimers colored differently. (**b**) McsB is a self-compartmentalized kinase, as shown in the half-cut surface representation. The location of the active sites within the phosphorylation chamber is highlighted in lilac and the pArg194 clamp in orange. The right panel illustrates the high conservation of the respective active site and interface regions. (**c**) Orthogonal view into the octamer (cross section indicated), with the pArg194

residue highlighted in orange. The right panel illustrates the binding of pArg194 in a
565 complementary charged pocket of the neighboring subunit (top) and its Fo-Fc omit density calculated at 2.5 Å resolution and contoured at 3.0 σ (bottom). (**d**) Structural details of pArg194 bound to the pR-RS site of a molecular neighbor.

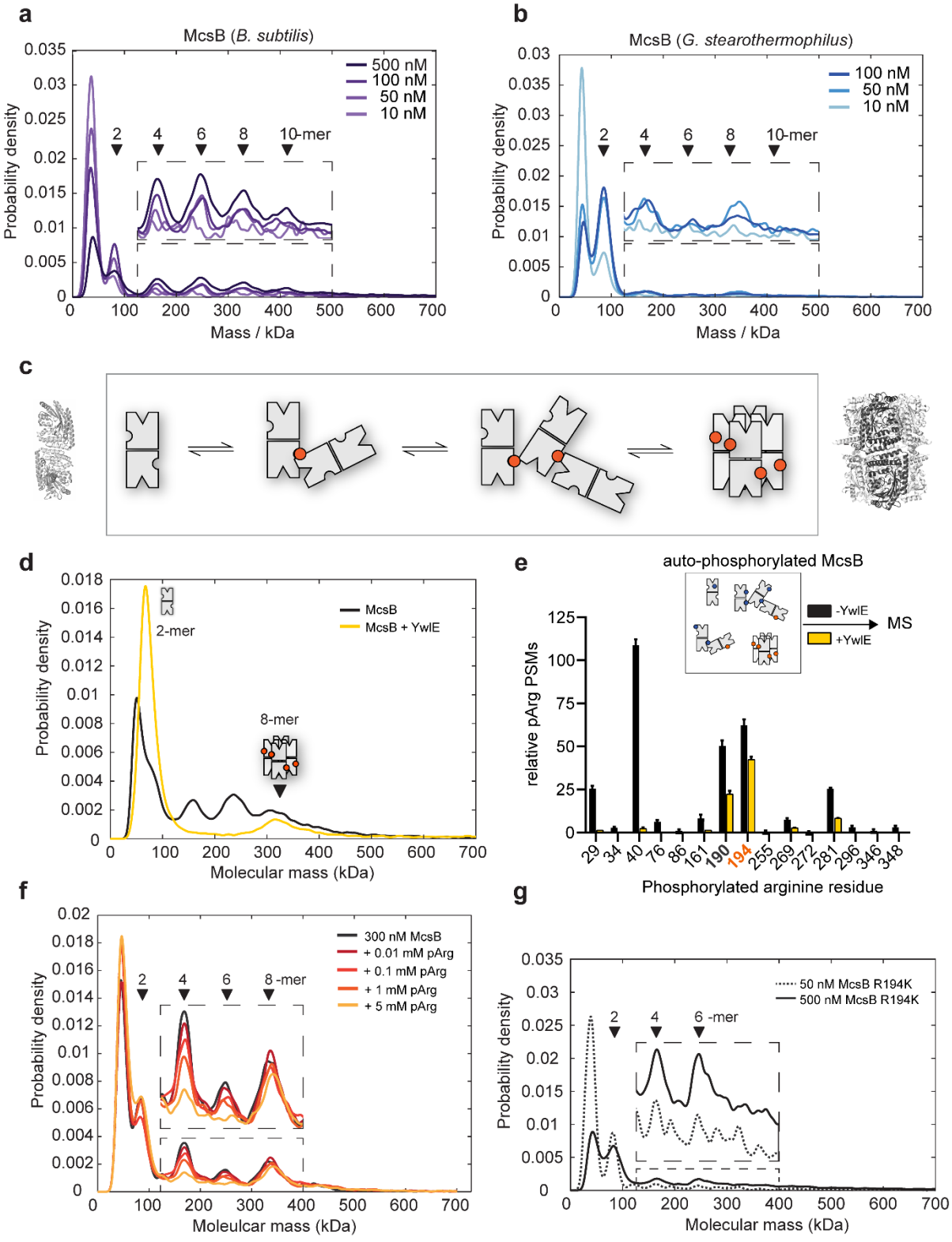

570

Figure 3: McsB$_{BS}$ oligomer conversion depends on a phospho-arginine switch.

(**a**) Distribution of McsB$_{BS}$ oligomers at increasing protein concentrations (10 to 500 nM). (**b**) Distribution of McsB$_{GS}$ at increasing protein concentration (10 to 100 nM). (**c**) Proposed model of McsB oligomer conversion, with pArg residues represented by

colored circles. Structural data are present for dimer and octamer. (**d**) Mass photometric analysis of the effect of the YwlE phosphatase on $McsB_{BS}$ oligomer conversion. (**e**) MS data showing that all pArg residues of autophosphorylated McsB are quantitatively removed, except pArg190 and pArg194. (**f**) Mass photometric analysis of the effect of free pArg on $McsB_{BS}$ oligomer conversion. (**g**) Mass photometric analysis of the R194K mutant, showing selective destabilization of the octamer. Size markers are indicated.

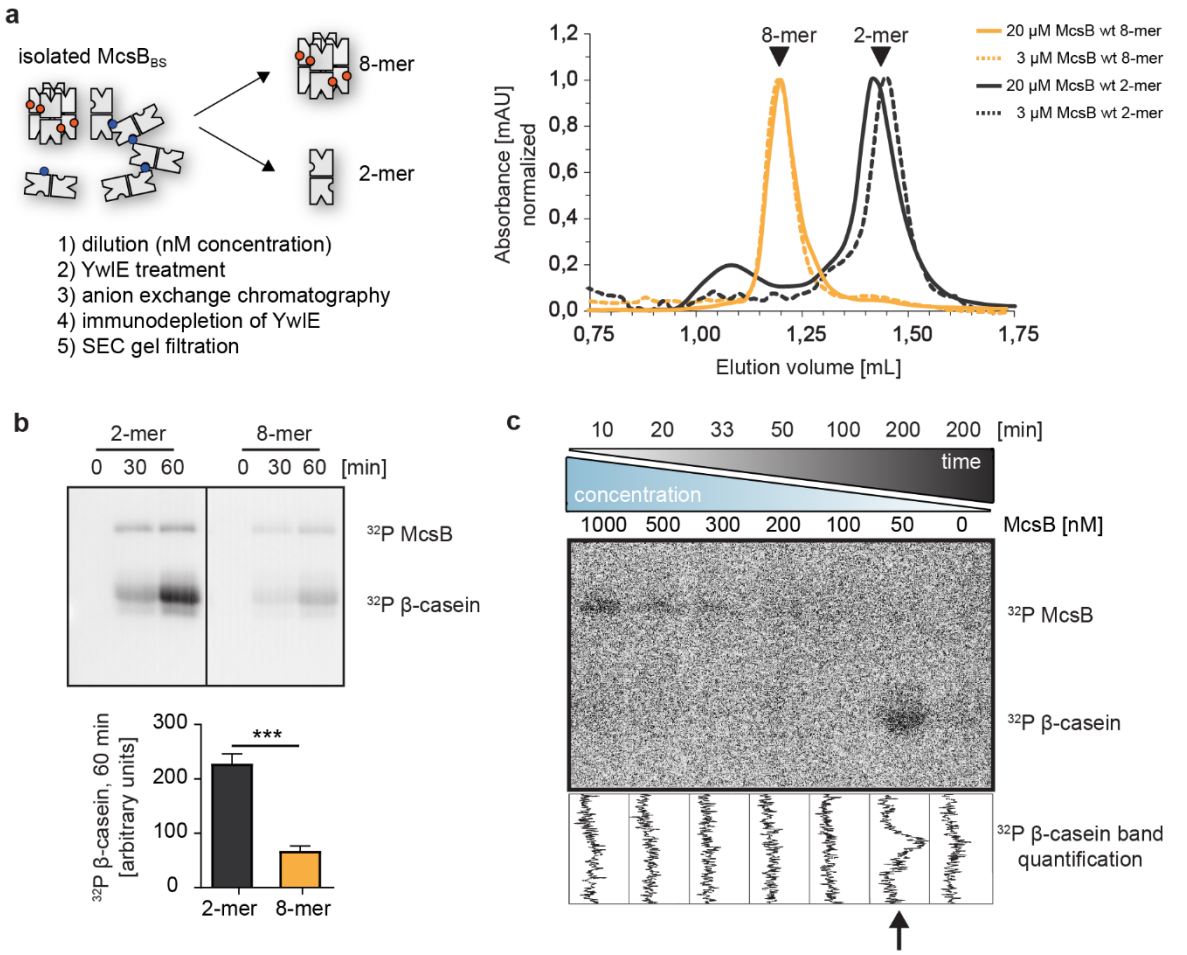

585

Figure 4: McsB$_{BS}$ dimer and octamer exhibit distinct kinase activities.

(**a**) Outline of preparing dimeric and octameric McsB$_{BS}$ (left panel). The established procedure efficiently reconstituted the two *B. subtilis* kinase forms, as seen in the SEC profiles of the separated McsB$_{BS}$ samples (right panel). (**b**) Radiometric ^{32}P kinase
590 assays visualizing the activity of dimeric and octameric McsB$_{BS}$ (1 µM) against β-casein (55 µM). ***P≤ 0.001; two-tailed unpaired t test. n=3 (independent reactions). Error bars indicate SD (**c**) Radiometric kinase assays using an McsB dilution series. To account for the different enzyme amounts (1000-50 nM), assays were incubated for different times (10-200 minutes).

595

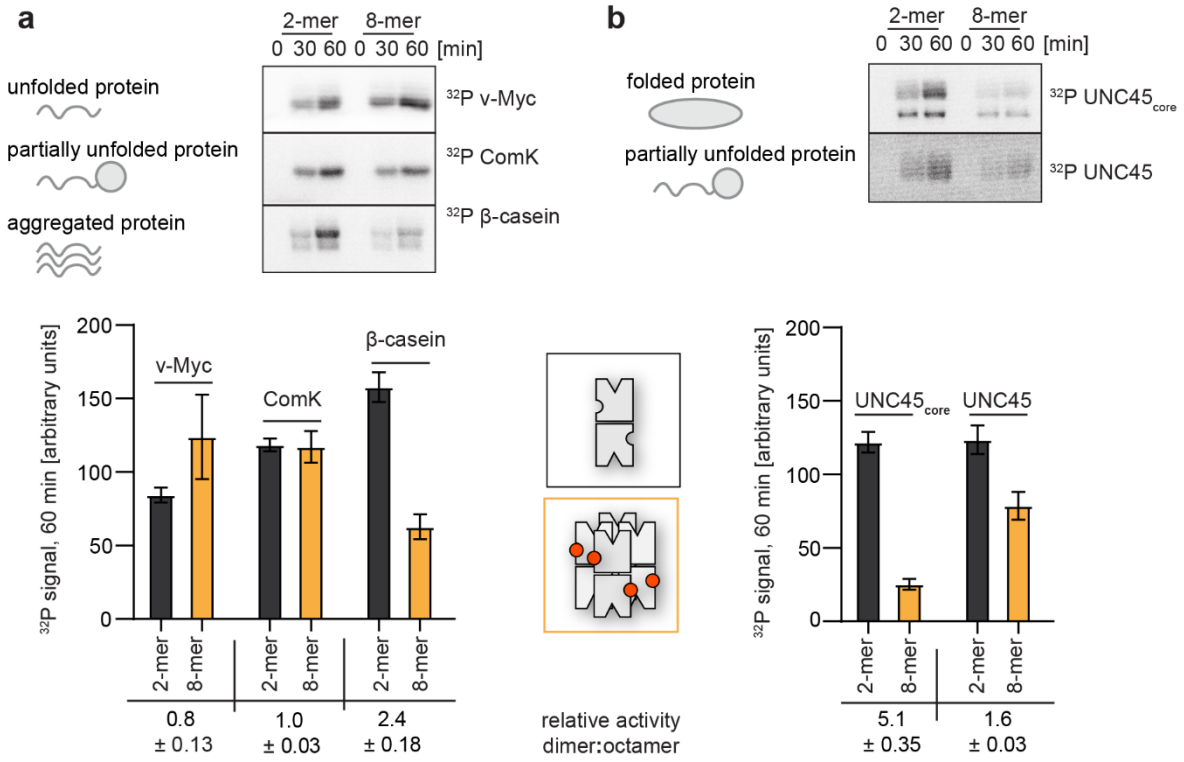

Figure 5: A switch in oligomeric state causes a switch in substrate selectivity.

(**a**) Radiometric assays of dimeric and octameric $McsB_{BS}$ using different model substrates. A plot of the quantified activities of dimer (black) and octamer (orange) in the lower panel highlights the distinct substrate preferences. Relative activity as mean ± SD. n=3 (independent reactions). Error bars indicate SD (**b**) Kinase assay using the model substrate UNC-45 confirms the substrate filtering role of the octameric cage (top, raw data; bottom, quantification of ^{32}P signal). Relative activity as mean ± SD. n=3 (independent reactions). Error bars indicate SD.

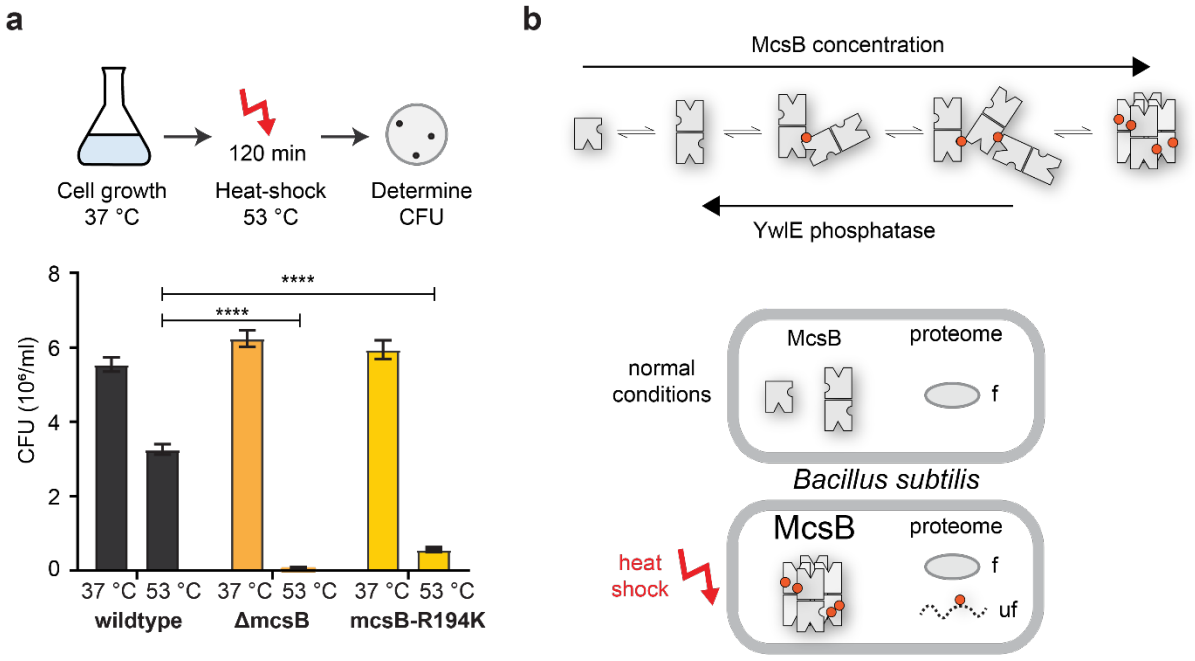

Figure 6: Octamer formation of McsB is critical for the heat-shock response.

(a) *In vivo* analysis of the R194K McsB oligomerization mutant. Compared to wildtype *B. subtilis* cells, ΔmcsB and R194K mutant cells exhibit a strong thermo-sensitive phenotype. ****P≤ 0.0001; one-way ANOVA and Tukey's multiple comparison test of heat-shocked samples. n=5 (biological independent samples). Error bars indicate SD **(b)** Proposed model illustrating how McsB protein concentration and YwlE activity shape the distribution of McsB oligomers. pArg phospho marks are indicated by red spheres. As shown below, monomer and dimer are prevalent under non-stress conditions. Presumably, their activity on folded proteins (f) can be reversed by the arginine phosphatase YwlE. Under heat-shock, McsB and other components of the stress response machinery are strongly enriched, favoring formation of octameric particles that selectively target misfolded (uf) proteins.

METHODS

Protein Expression and Purification

For production of recombinant McsB (*B. subtilis* and *G. stearothermophilus*) and the YwlE phosphatase from *G. stearothermophilus*, we used constructs and procedures described previously[20,27]. In general, protein expression was performed in *Escherichia coli* BL21(DE3) grown in LB-medium supplemented with 50 µg/ml ampicillin. Cultures expressing McsB from *B. subtilis* and mutated variants thereof were grown to an OD_{600} of 1.0 at 37 °C, shifted to 18 °C and expression was induced upon addition of 0.5 mM IPTG. Cells were harvested after overnight expression and the pellet was resuspended in 50 mM Tris-HCl pH 7.5 and 50 mM NaCl. All proteins were purified by Ni-NTA affinity chromatography using a 5 ml HisTrap column (GE Healthcare Life Sciences) equilibrated with 50 mM Tris-HCl pH 7.5 and 150 mM NaCl. Bound proteins were eluted with the equilibration buffer supplemented with 250 mM imidazole. Subsequently, the proteins were loaded on a Superdex 200 16/60 column (GE Healthcare Life Sciences) equilibrated with 20 mM Tris-HCl pH 7.5 and 50 mM NaCl. Proteins were concentrated using 30 kDa cut-off Vivaspin columns (Sartorius) and their concentration was determined by their absorbance at 280 nm.

Mutagenesis

Site-directed mutagenesis of McsB from *B. subtilis* expression constructs was performed using the Q5 Site-Directed Mutagenesis Kit (New England BioLabs) following the manufacturer's procedures. Primers are listed in Supplementary Table 2. The mutation in the *mcsB* locus was introduced into the chromosome of strain *Bacillus subtilis* 168 $mcsB_{R194K}$ as described in[20], using the mutagenesis primer given in **Supplementary Table 2**.

Isolation of dimeric and octameric McsB from *B. subtilis*

The wild type protein was expressed and initially purified as described above. However, after the Ni-NTA purification the McsB protein (5 mg/ml in 15 ml) was dephosphorylated upon addition of 1 µM of YwlE on ice for 30 minutes. The sample

was loaded on a 6 ml Resource Q column (GE Healthcare Life Sciences) equilibrated with 50 mM HEPES-NaOH pH 7.5 and 50 mM NaCl. Dimeric and octameric McsB were separated in a linear gradient to 500 mM NaCl. Residual YwlE was removed by immuno-depletion using an YwlE antibody[40] immobilized on Protein A Dynabeads (Thermo Scientific). The separated oligomeric species were further purified using a Superdex200 10/30 column equilibrated with 50 mM HEPES-NaOH pH 7.5 and 50 mM KCl.

Analytical size exclusion chromatography

Analytical size exclusion chromatography was performed over a Superdex 200 3.2/300 increase column equilibrated with 50 mM HEPES-NaOH pH 7.5, 50 mM KCl using an Ettan LC system (GE Healthcare Life Sciences). Expected molecular masses were calculated based on the separation of the gel filtration standard (Bio-Rad) by the column.

Radiometric kinase assay.

An aliquot of the McsB kinase (1 µM) was incubated with 12 µM substrate at 37 °C in a buffer containing 50 mM HEPES-NaOH pH 7.5, 50 mM KCl, 2 % *(v/v)* glycerol, 10 mM β-mercaptoethanol, 7.5 mM $MgCl_2$, 5 mM cold ATP and 50 µCi γ-32^P ATP (Hartmann Analytics). Reactions were quenched at given timepoints upon addition of 5x SDS sample buffer and resolved on a Tris-glycine SDS-PAGE. Gels were dried, exposed to a phosphor imaging plate (BAS-MS 2025, Fuji film) overnight and visualized with a Typhoon Biomolecular imager (GE Healthcare). Intensities were determined by densitometry using ImageJ (version 1.47).

Heat-shock assay

A preculture of *B. subtilis* 168 was grown in LB-medium to stationary phase at 37 °C overnight. 5 ml were used to inoculate 25 ml LB-medium and the culture was grown to an OD_{600} of 0.5 in duplicates. To evoke a heat-shock, one culture was mixed with 25 ml LB-medium at 53°C and incubated at 53°C for additional 2 hours. The second culture was mixed with 25 ml of LB-medium at 37 °C and incubated at room

temperature for 2 hours. Cells from both cultures were pelleted, flash frozen in liquid nitrogen, thawed, and resuspended in 500 µL of 50 mM Tris-HCl pH 7.5, 50 mM NaCl supplemented with 250 µg Lysozyme (Sigma), 5 µg DNase I (Roche) and 1x complete Protease Inhibitor Cocktail (Roche). The suspensions were sonicated for 2 minutes on ice. The lysate was cleared by centrifugation, the total protein concentration was adjusted to 1.8 mg/ml using Bradford reagent (Bio-Rad) and 1 ml aliquots were separated over a Superdex 200 16/60 equilibrated with 20 mM Tris-HCl pH 7.5 and 50 mM NaCl. Fractions of 1.5 ml were collected from which proteins within 1 ml were precipitated with 200 µL cold saturated TCA solution and incubated on ice for around 15 hours. The fractions were washed two times with ice-cold acetone and left drying. Each pellet was resuspended in 30 µL of SDS-PAGE sample buffer and separated on a 4-12 % Bis-Tris SDS-PAGE gel (NuPAGE) using 1x MES running buffer (NuPAGE). Immunoblotting was performed using anti-McsB antibody following standard procedures. Standards used during size exclusion chromatography experiments of cell lysates were composed of 71 µM dimeric McsB *G. stearothermophilus* (dimer) and 71 µM oligomeric McsB from *B. subtilis* purified as described above.

Cell viability assay

A preculture of each *B. subtilis* 168 strain (WT vs. *ΔmcsB* (1) vs $mcsB_{R194K}$) was grown in LB-medium to stationary phase at 37 °C degrees overnight. 6 ml modified synthetic medium[41] (50 mM Tris-HCl pH 7.5, 15 mM $(NH_4)_2SO_4$, 8 mM $MgSO_4$, 27 mM KCl, 7 mM Na-citrate, 0.6 mM KH_2PO_4, 2 mM $CaCl_2$, 1 µM $FeSO_4$, 10 µM $MnSO_4$, 4.5 mM K-glutamate, 0.20% *(v/v)* glucose, 100 µM L-Trypthophan) was inoculated with the preculture to an OD_{600} of 0.05 and grown to 0.4. Each culture was split into halves and one part was transferred to 53 °C to evoke heat stress while the other half was kept at room temperature for 2 hours. After the heat-shock, the cultures were diluted 1:1000 using synthetic medium. 50 µL of culture were withdrawn and plated on pre-warmed LB-agar plates and colony forming units (CFU) were determined using ImageJ (version 1.47).

Crystallization and Structure Determination

Octameric $McsB_{BS}$ was crystallized in a hanging drop, vapor diffusion setup at 100 mg/ml concentration using 200 mM of Mg-acetate as reservoir solution. Crystals were grown at 4 °C and transferred into a solution containing PEG400 and mother solution in a ratio of 4:6 for cryo-protection, crystals were harvested and flash-cooled in liquid nitrogen. X-ray diffraction data were collected at the beamline X06SA at the Swiss Light Source (Villigen-PSI, Switzerland). Diffraction data were processed and scaled using the XDS package[42] to a resolution of 2.5 Å. Initial phases were obtained by Molecular Replacement using PHASER[43] and the structure of $McsB_{GS}$ (6FH1) as starting model[20]. The model was improved in iterative cycles of manual building using COOT[44] and refinement with Phenix[45] omitting 5 % of randomly selected reflections for calculation of R_{free}. Model quality was monitored using MolProbity[46] and the final model exhibited good stereochemistry with 98 % of residues in favored regions of the Ramachandran plot and without any outliers.

Statistical analysis

Data analysis and statistical calculations of the cell viability assay and radiometric kinase assay were performed in GraphPad Prism 8. Other data analysis was performed in Excel (Microsoft) if not stated otherwise. Excel (version 2013, Microsoft) was used for graph preparations and they were further modified in Illustrator (version 2020, Adobe).

Mass spectrometry of McsB

McsB from *B. subtilis* (1 mg/ml) was incubated in triplicates in the presence or absence of 0.2 mg/ml YwlE from *G. stearothermophilus* in 50 mM Tris-HCl pH 7.5, 50 mM NaCl at 37 °C for 1 hour in a final reaction volume of 100 µl. 2 mM Vanadate (Sodium Orthovanadate, NEB, pre-incubated for ten minutes at 95 °C to dissociate Vanadate oligomers) was added to each reaction to inhibit the YwlE phosphatase. The samples were reduced with 10 mM DTT at 37 °C for 60 minutes and alkylated with 30 mM methyl methanethiosulfonate (MMTS) at room temperature for 45 min. After addition of MMTS, the pH was immediately adjusted to ~7 by addition of 1 M HEPES-NaOH pH 7.2. Samples were digested with 2.5 µg of Trypsin Gold (Mass Spectrometry

Grade, Promega, solubilized to 1 µg/ul in 50 mM Acetic Acid) overnight at 37 °C. Directly after addition of Trypsin, the pH was adjusted as above.

For LC-MS Analysis, an UltiMate 3000 RSLC nano system was coupled to an Orbitrap FusionLumosTribrid mass spectrometer (Thermo Fisher Scientific). Tryptic peptides were loaded onto a trap column (PepMap C18, 5 mm × 300 µm ID, 5 µm particles, 100 Å pore size, Thermo Fisher Scientific) at a flow rate of 25 µL/min using 0.5% acetic acid (pH 4.5 with NH_4OH) as mobile phase to prevent pArg hydrolysis during the removal of salts in the precolumn[15]. After 10 min, the trap column was switched in line with the analytical column (PepMap C18, 500 mm × 75 µm ID, 2 µm, 100 Å, Thermo Fisher Scientific). Peptides were eluted by a binary gradient of buffer A and B over a period of 60 min (From 98% A (0.1% (v/v) formic acid) and 2% B (80% (v/v) acetonitrile/0.08% (v/v) formic acid) to 35% B) with a flow rate of 230 nl/min. After electrospray ionization (EASY-Spray source (Thermo Fisher Scientific), the MS was operated in data-dependent mode, using a full scan (m/z range 380-2000, nominal resolution of 120,000, target value $4x10^5$) followed by MS/MS scans using an Orbitrap resolution of 30,000 with 3 seconds cycle time (isolation width 1.2 m/z, mass tolerance 10 ppm). Precursor ions selected for fragmentation (excluding charge state 1, 7, 8, >8) were put on a dynamic exclusion list for 10 s and minimum intensity threshold for precursor selection was set to $2x10^4$. Collision Induced Dissociation with 30% normalized collision energy was used for fragmentation. Additionally, the AGC target was set to $2x10^5$ and the maximum injection time was set to 250 ms.

Raw data were extracted using Proteome Discoverer (version 2.3.0.523, Thermo Scientific) and searched with MS Amanda 2.0[47] against a combined database of *E. coli* strain BL21(DE3) UniProt Reference Proteome with common contaminants and the respective sequences of *B. subtilis* McsB and *G. stearothermophilus* YwlE added. Methylthio-modification of cysteine was set as a fixed modification. Phosphorylation of serine, threonine, tyrosine, and arginine, oxidation of methionine and deamidation of asparagine and glutamine were set as dynamic modifications. Because tryptic cleavage is impaired at phosphorylated arginine, a maximum of three missed cleavage sites was allowed. The peptide mass deviation was set to 5 ppm; fragment ion mass deviation to 0.02 Da. MS Amanda score was filtered for >150 and the percolator[48] was used to filter for PEP < 0.01. All phosphopeptide hits were automatically reanalyzed by phosphoRS[49] for reliable phosphorylation site analysis (threshold for localization

probability > 90%). Quantitative information of McsB peptide spectrum matches (PSMs) was obtained by spectral counting, summing up all spectra associated with a specific match and applying a scaling factor for each sample to each PSM by adjusting the values to normalized spectral counts and subsequently used to determine the relative pArg phosphopeptide spectral counts. The graph depicts the mean of the normalized triplicate measurements (with standard deviation).

iSCAT setup and mass photometry assay

The mass photometry experiments were performed on a custom-built iSCAT microscope similar to the one described in[28,50] with a 445 nm laser diode (Lasertack). Coverslips were cleaned by sequential bath sonication in H_2O, isopropanol and H_2O for 5 min each. They were then rinsed with H_2O, blow-dried in a nitrogen stream and assembled into flow chambers[51]. Proteins were diluted into McsB Buffer (20 mM Tris-HCl pH 7.5, 50 mM NaCl) and incubated at room temperature for at least 2 h in the absence or presence of other compounds (free phospho-arginine, phosphorylated peptide etc. as stated). The flow chambers were loaded with buffer to find a clean area and the optimal focus position, defined as the z-position with maximum root-mean-square deviation of the signal from the glass surface pattern. Subsequently, 20 µL of the protein sample were flushed through the flow chamber and landing was recorded at a frame rate of 1 kHz. The videos were saved with 2 frames averaged and 3 pixels x 3 pixels binned to their mean to give an effective frame rate of 500 Hz and to reduce the file size. The effective pixel size after binning was 70.2 nm.

Mass photometry data analysis procedure

The videos of proteins binding to the glass surface were analysed with the software DiscoverMP (version 2.1.0, Refeyn Ltd). The software detects binding events and determines the respective interferometric scattering contrasts. The user can choose how many frames are averaged for continuous background removal (navg) and can set the thresholds T1 and T2 for the two image filters, which are used to detect the binding events. Filter 1 is based on T-tests of the pixel intensity fluctuations. As a protein binds to the glass, the pixel intensity changes suddenly. This change is associated with an increase of the filter 1 score calculated as –ln(p), where p is the p-

value of the T-test comparing pixel values at navg frames before and navg frames after the event. The smallest intensity jump amplitude that exceeds random noise fluctuations and is associated with a binding event is controlled by the value of threshold T1. The signatures of the binding events in interferometric images are radially symmetric. Filter 2 measures the radial symmetry of all pixel neighbourhoods of the interferometric images[52]. The lowest symmetry score expected at the centre of a peak is defined as threshold T2. Pixel clusters that exceed both thresholds T1 and T2 are used for peak fitting. The amplitude of the peak fit provides an estimate for the interferometric peak contrast. The peak signature (point spread function) is modelled as a superposition of two Sombrero functions multiplied by two Gaussians. The small size of McsB monomers of only 42 kDa made it difficult to detect landing molecules of this species quantitatively above the baseline noise. To determine the optimum filter thresholds (T1 and T2) for the detection of these species and an estimate of the percentage of detected particles, we generated a semi-synthetic movie that used frames from a video recorded with McsB Buffer alone to simulate an experimental background and added simulated point spread functions as landing events that had the expected scattering contrast of a 42 kDa protein (contrast = 2.2×10^{-3}). The point spread function was modelled as a superposition of two sombrero functions that is convolved with two Gaussian smoothing kernels. This function was the same function used to fit experimental landing events. We then varied navg as well as T1 and T2, ran the analysis procedure, and determined the number of true positive and false positive detections. To determine the maximum number of true positive detections possible at the respective signal-to-noise ratio, we simulated 1000 frames with 100 landing events that were not allowed to overlap closer than 12 pixels spatially and 26 frames temporally. Based on this control simulation, we chose navg = 21, T1 = 1.2 and T2 = 0.15 to process the experimental videos. Using these parameters, the number of true positive detections of monomers in the simulation was 57.2 ± 4.0% (mean ± standard deviation of 5 simulations) and the number of false positive detections was 12.2 ± 3.0%. For dimers (contrast = 4.3×10^{-3}), a simulation with the same parameters gave 92.2 ± 3.0% true positive detections and 3.8 ± 1.6% false positive detections. The interferometric scattering contrast was converted into molecular mass by calibration with standard proteins (here: protein A – 42 kDa, alcohol dehydrogenase dimer and tetramer – 73.5 and 147 kDa, β-amylase dimer and tetramer – 112 and 224 kDa). Their interferometric scattering contrast was plotted as

a function of mass and a line was fitted to the resulting graph (**Extended Data Fig. 6**). The slope (5.023×10^{-5} kDa^{-1}) and intercept (1.261×10^{-4}) of the calibration line were used to convert contrast into mass according to mass = (contrast – intercept) / slope.

835

Extended Data Figures

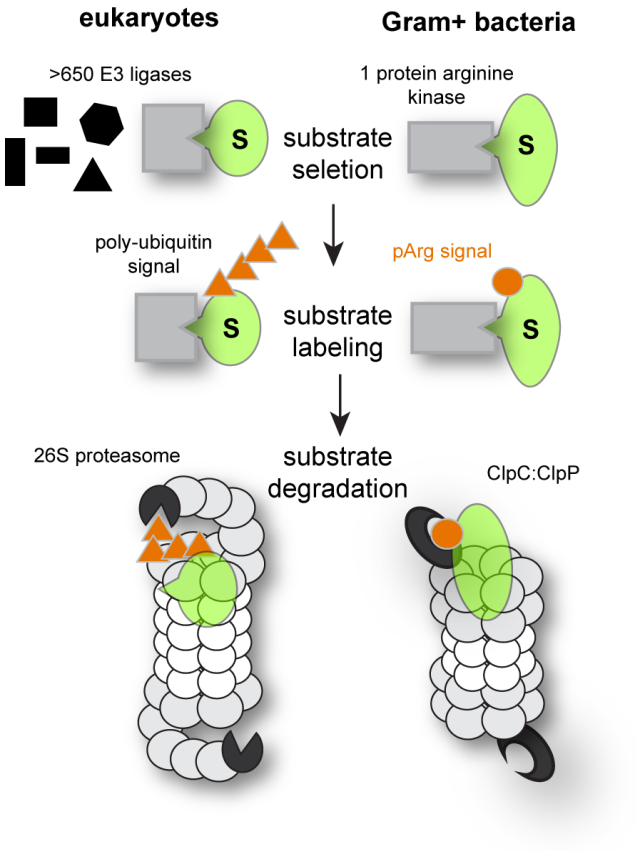

840

Extended Data Figure 1: Degradation pathways in comparison. Comparison of the ubiquitin-proteasome and pArg-ClpCP degradation pathways that are similarly organized but use distinct degradation signals (orange).

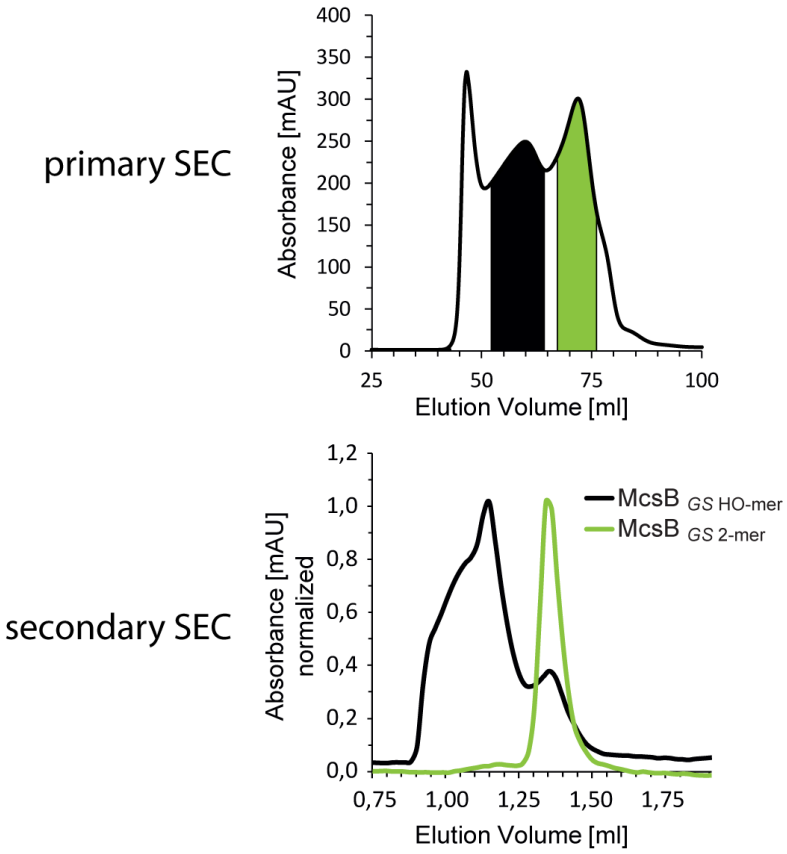

Extended Data Figure 2: Higher order oligomers of McsB$_{GS}$. SEC chromatogram of recombinant McsB$_{GS}$ showing two dominant peaks (top panel). Secondary SEC runs of the two major peaks (bottom panel).

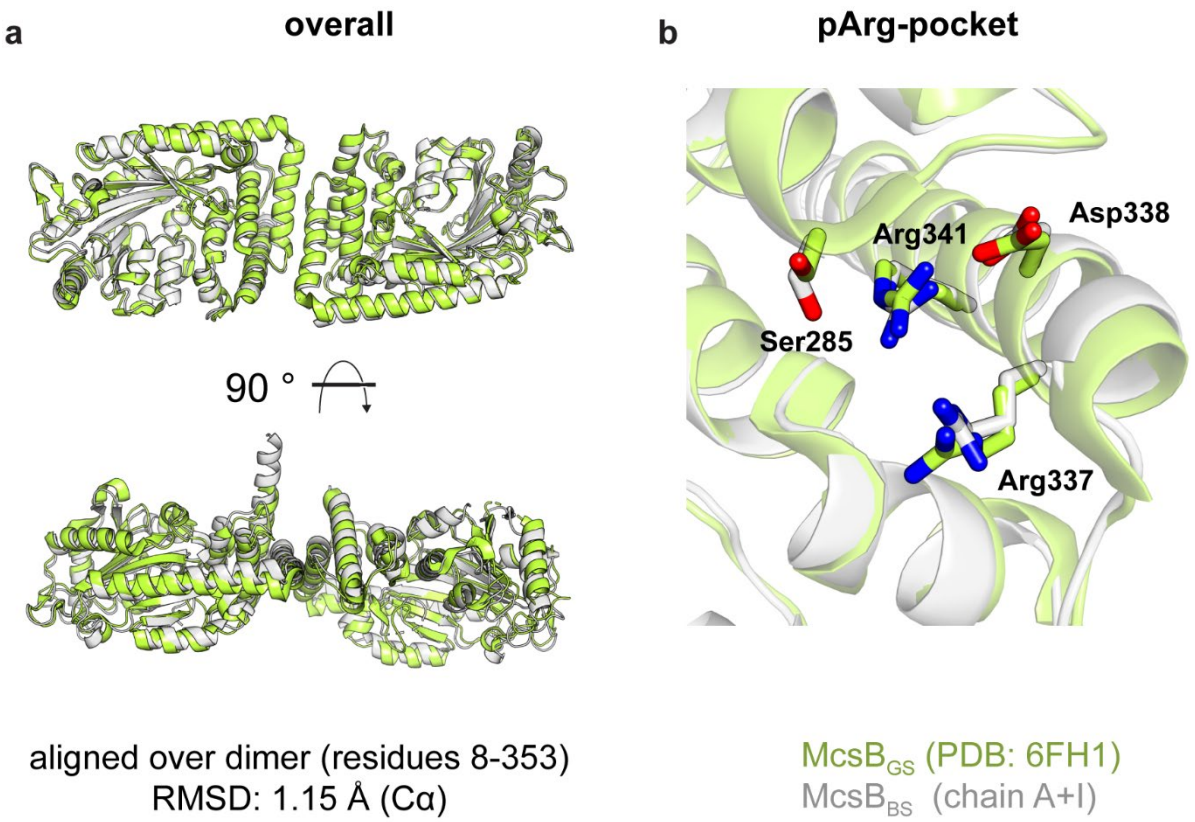

855 **Extended Data Figure 3: Comparison of McsB$_{BS}$ and McsB$_{GS}$.** (**a**) Structural alignment of the functional dimer (left) and the pArg binding pocket (right). The two orthologs are colored differently.

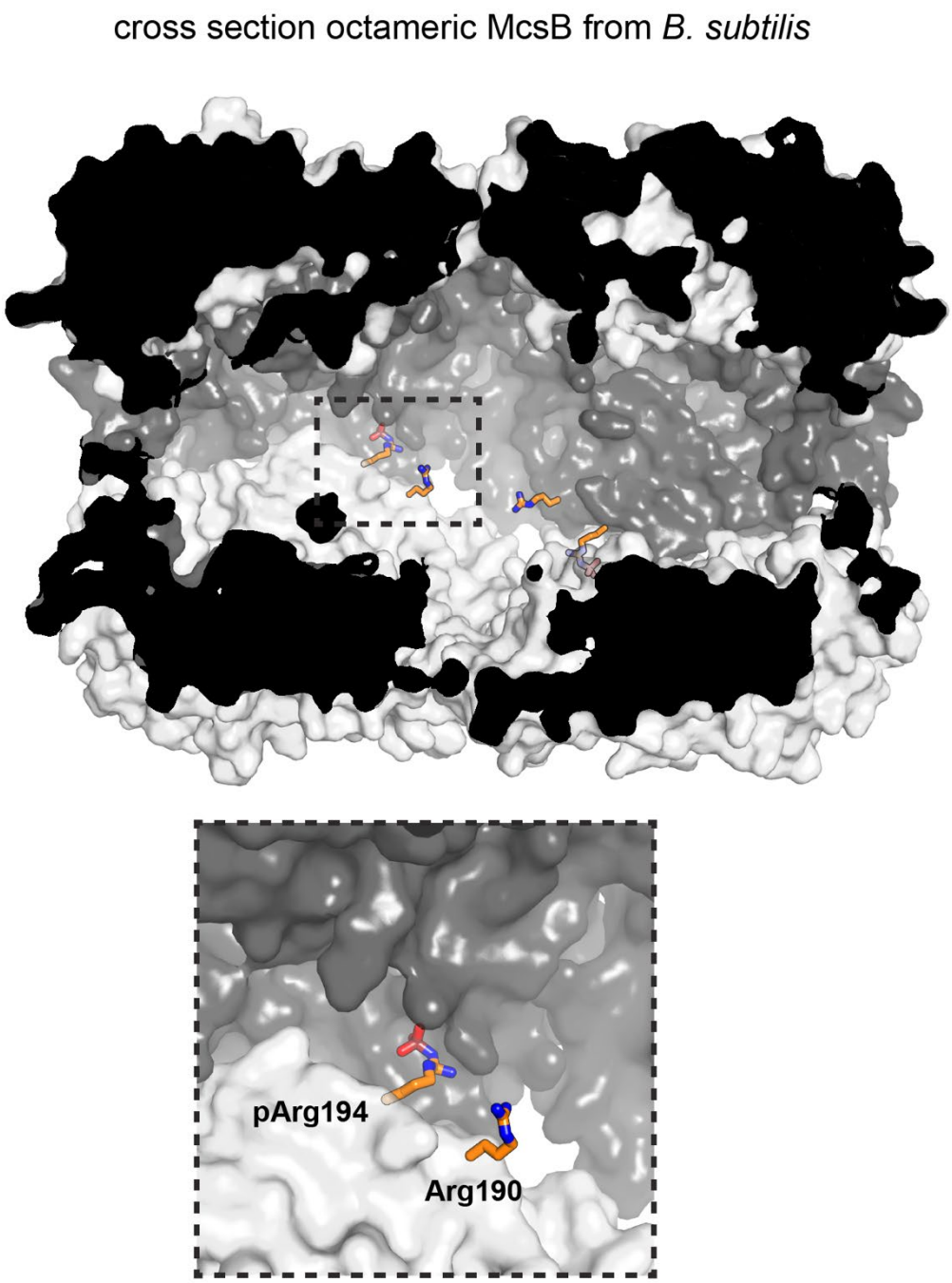

860

Extended Data Figure 4: Shielding of pArg190 and Arg194 in the dimer-dimer interface. The surface plot shows a half-cut particle (semi-transparent surface), highlighting the burial of residues 190 and 194 in the octameric cage. Other auto-
865 phosphorylated arginine residues shown in **Fig. 3e** are surface exposed and thus accessible to YwlE.

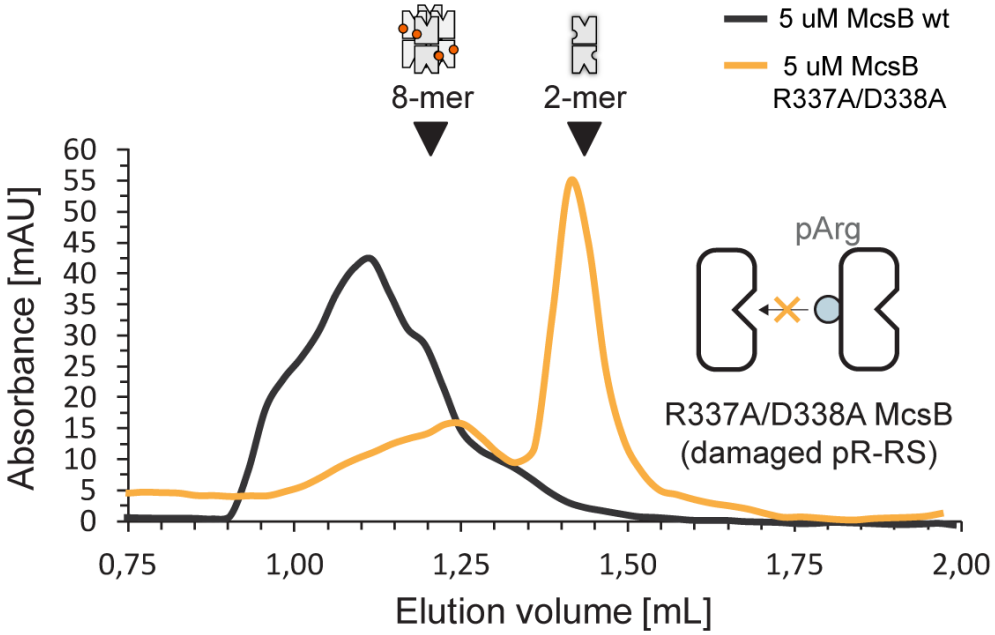

870 **Extended Data Figure 5: pArg-binding deficient mutant R337A/D338A.** SEC analysis of the pArg-binding deficient mutant R337A/D338A that mainly exists as a dimer. Size markers are indicated.

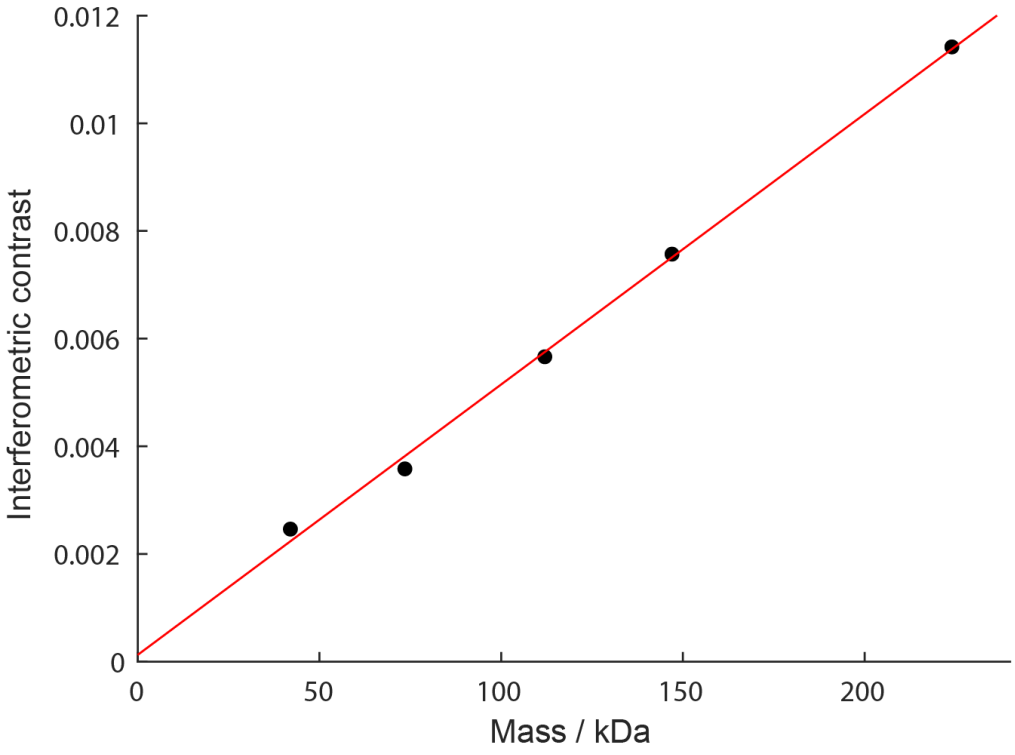

875

Extended Data Figure 6: Correlation of interferometric contrast and molecular mass. The interferometric contrast signal of landing molecules was converted into molecular mass based on the signal of standard proteins with known mass (here: protein A – 42 kDa, alcohol dehydrogenase dimer and tetramer – 73.5 and 147 kDa, β-amylase dimer and tetramer – 112 and 224 kDa).

880

Source Data Figures: Uncropped gels

885

Figure 2c

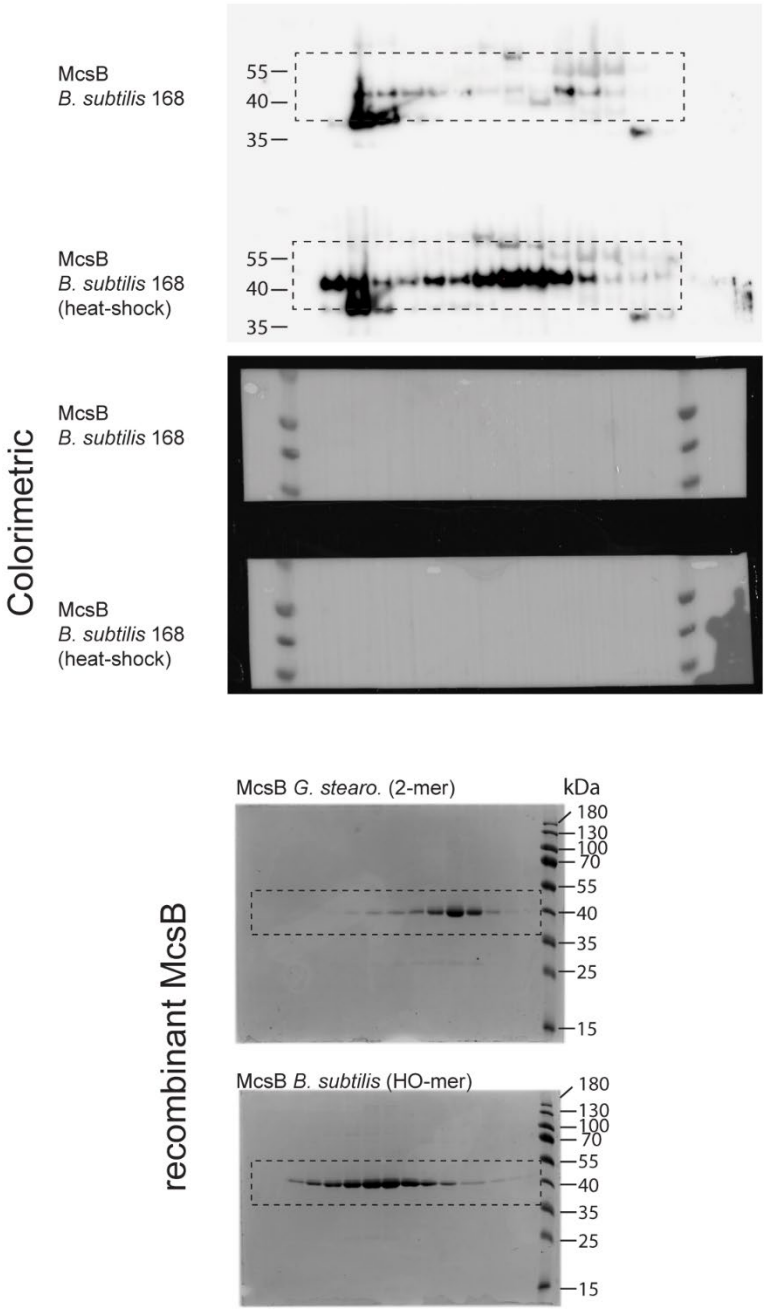

Figure 4b

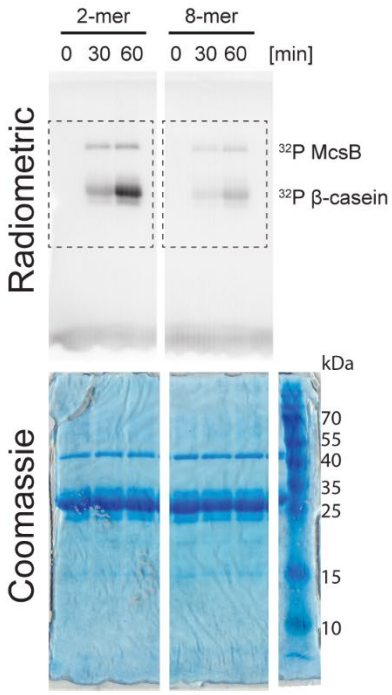

Figure 5a

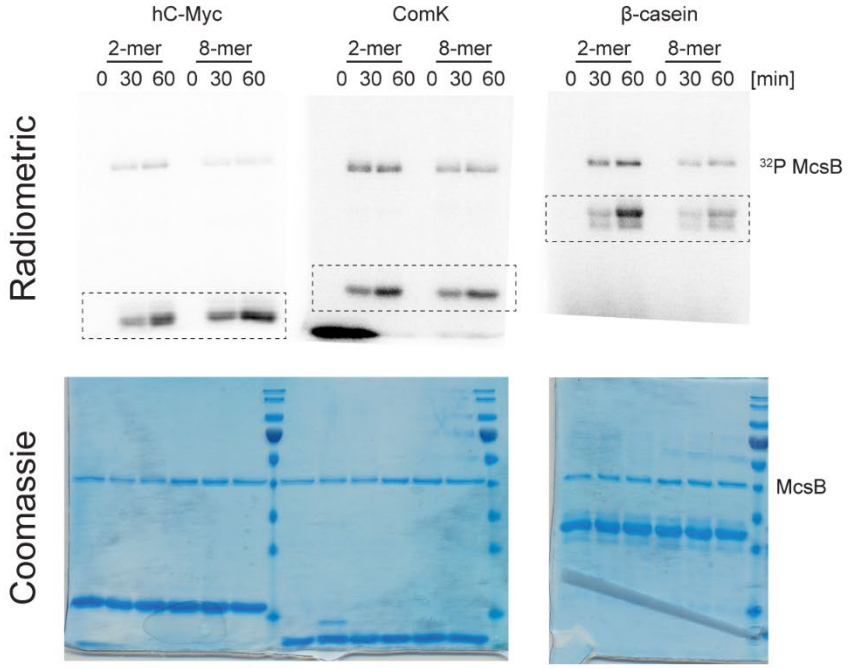

Figure 5b

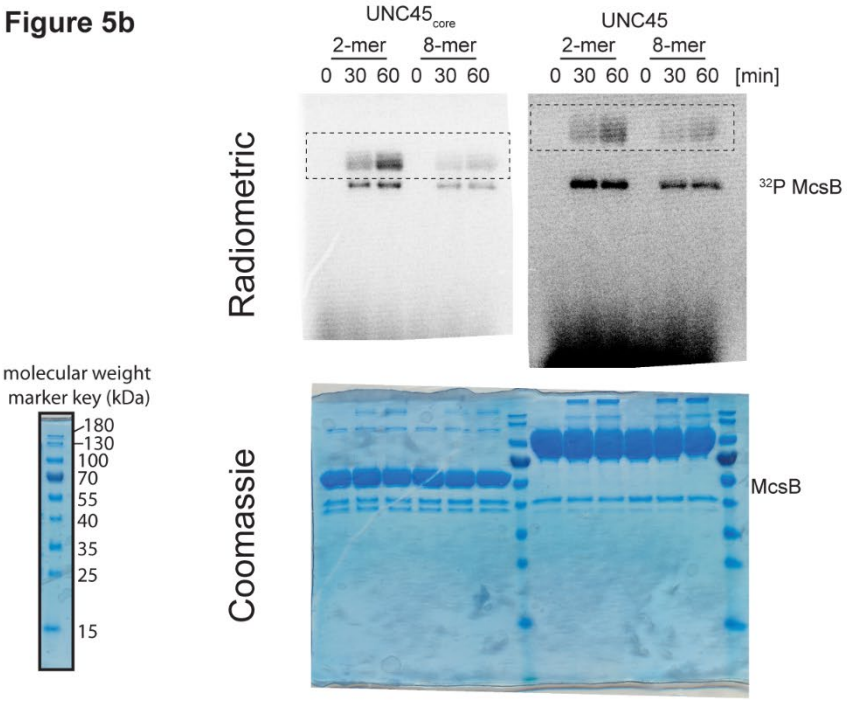

Figure 5d

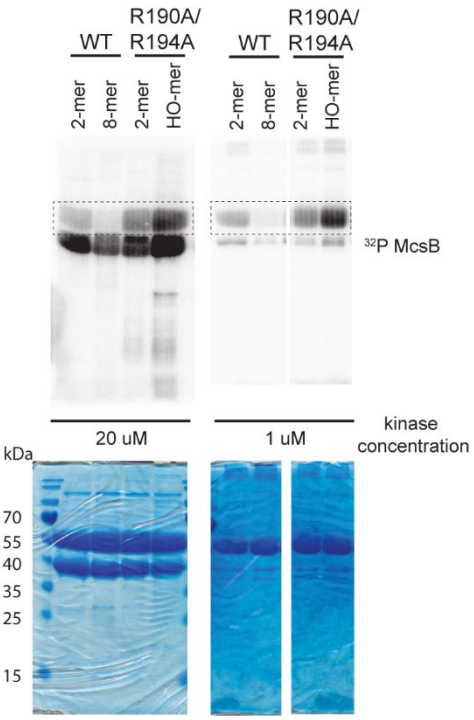

890

SUPPLEMENTAL VIDEOS

Supplemental Video 1: Illustration of the structural organization of the McsB$_{BS}$ octamer, which forms a self-compartmentalized protein kinase. The video introduces the basic building block, the McsB dimer, showing the location of the active site and the pArg clamp. After assembling the McsB octamer, the surface presentation emphasizes the self-compartmentalization of the protein kinase, locking the active sites within a phosphorylation chamber. Narrow entry gates restrict access of substrate allowing the selective degradation labeling of unfolded proteins or protein segments.

SUPPLEMENTAL TABLES

Supplemental Table S1: Data collection and refinement statistics.

	Octameric $McsB_{BS}$ (6TV6)
Space group	$P2_12_12$
Cell dimensions	
a, *b*, *c* (Å)	137.79, 147.64, 81.47
α, *β*, *γ* (°)	90, 90, 90
Resolution (Å)[a]	49 – 2.5 (2.56 – 2.5)
$R_{meas(I)}$	0.146 (1.53)
I/σ (I)	13.2 (1.2)
$CC_{1/2}$	0.998 (0.561)
Completeness (%)	99.8 (99.8)
Redundancy	6.7 (6.9)
Resolution (Å)	49 – 2.5
No. reflections	58,139
R_{work} / R_{free}	0.193 / 0.237
No. atoms	
protein	11,289
ion	4
water	117
B factors	
protein	55.6
ion	57.7
water	51.4
R.m.s. deviations	
Bond lengths (Å)	0.009
Bond angles (°)	1.083

[a]Values in parentheses are for highest-resolution shell.

Supplemental Table S2: Primers used for site-directed mutagenesis

Plasmid	Forward primer	Reverse primer
pET21-mcsB$_{R337A/D338A}$-His6	GCCATTCGAAGAGCG GCTCTCATCAG	CGCTTCGTTCGGTCGCA AAGCGCC
pET21-mcsB$_{R190A/R194A}$-His6	TAAATGCAATTATACCGGCAAT TAATCA ATTAGGCTTAGTTGTTAG	TTTGCGCAGTTAAAACC AGCGCCGGCAGAT GCATCATGACCG
pET21-mcsB$_{R194K}$-His6	GATTAATTGCCGGTATAATTTT ATTTATTTGCCTAGTTAAAACC AGCGCCG	CGGCGCTGGTTTTAACT AGG CAAATAAATAAAATTATA CCG GCAATTAATC
pMAD-mcsB$_{R194K}$	ATTATACCGGCAATTAATCA	TTTATTTATTTGCCTAGT TAAAACC

910